Biomaterials 30 (2009) 622–631

Contents lists available at ScienceDirect

Biomaterials

journal homepage: www.elsevier.com/locate/biomaterials

Sequential delivery of dexamethasone and VEGF to control local tissue response for carbon nanotube fluorescence based micro-capillary implantable sensors

Jaeyun Sung [a], Paul W. Barone [a,c], Hyunjoon Kong [a,b], Michael S. Strano [c,*]

[a] Department of Chemical and Biomolecular Engineering, University of Illinois Urbana-Champaign, 600 S. Mathews Avenue, Urbana, IL 61801, USA
[b] Institute for Genomic Biology, University of Illinois Urbana-Champaign, 1206 W. Gregory Drive, Urbana, IL 61801, USA
[c] Department of Chemical Engineering, Massachusetts Institute of Technology, Building 66-566, 77 Massachusetts Avenue, Cambridge, MA 02139-4307, USA

ARTICLE INFO

Article history:
Received 1 July 2008
Accepted 23 September 2008
Available online 8 November 2008

Keywords:
Angiogenesis
Biosensor
Drug delivery
Immune response

ABSTRACT

In this study, we examined the *in vivo* pharmacological effects of the sequential delivery of dexamethasone (DX) followed by vascular endothelial growth factor (VEGF) on the immune response and localized vascular network formation around a hydrogel-coated, micro-capillary implant for single-walled carbon nanotube based fluorescence sensors. We demonstrate, for the first time, imaging of an SWNT fluorescence device implanted subcutaneously in a rat. For tissue response studies, the chick embryo chorioallantoic membrane (CAM) was used as a tissue-model for an 8-day implantation period. The average vascular density of the tissue surrounding a hydrogel-coated microdialysis capillary sensor with simultaneous, sequential, or no delivery of DX and VEGF was $1.24 \pm 0.35 \times 10^{-3}$ vessels/μm^2, $1.15 \pm 0.30 \times 10^{-3}$ vessels/μm^2 and $0.71 \pm 0.20 \times 10^{-3}$ vessels/μm^2, respectively. Calculation of the therapeutic index (vasculature/inflammation ratio), which reflects promotion of angiogenesis versus the host immune response, demonstrates that sequential DX/VEGF delivery was 60.3% and 139.3% higher than that of VEGF and DX release alone, respectively, and was also 32.1% higher when compared to simultaneous administration, proving to be a more effective strategy in utilizing the pharmacological impact of DX and VEGF around the biosensor-model implant.

1. Introduction

Recently, single-walled carbon nanotubes (SWNT) for use as near infrared (nIR) fluorescence based biomedical sensors have been developed [1–4]. Such sensors have advantages over conventional fluorescence sensors for use in *in vivo* applications. SWNT have tunable emission, from 900 to 1400 nm [5], in a region of the electromagnetic spectrum through which tissue and blood are most transparent while also exhibiting a low autofluorescent background signal [6]. Additionally, SWNT do not photobleach making them ideally suited as long-term sensors [7]. Previous work has demonstrated the specific detection of glucose [1], divalent metal cations [3] and DNA hybridization [4] even through blood and other highly scattering media [3]. The logical extension of such sensors, especially those aimed at glucose detection, is in use as miniaturized, implantable biosensors. However, the *in vivo* performance of biosensors capable of generating accurate and replicable real-time analyte measurements is often hampered by two major obstacles: the immune response to the sensor and limited transport of analytes [8,9]. Specifically, biosensors inside the body result in local inflammation in response to the trauma caused by the implantation process and foreign body recognition [10]. Subsequent protein adsorption and cell adhesion (biofouling), as well as fibroblast encapsulation-induced blood vessel regression, isolates the biosensor from the vasculature, resulting in limited analyte diffusion into the sensor [11–13]. These unfavorable physiological responses cause biosensors to progressively lose their accuracy and proper function within minutes to hours after implantation [11,14,15], and are therefore the main challenges in the widespread clinical use of *in vivo* biosensors.

Extensive efforts have been made in coating the biosensor surface with hydrogels to improve the biocompatibility and reduce biofouling and encapsulation effects [16–18]. The hydrogel coating has also been used as a drug depot for tissue response modifiers: dexamethasone (DX), an anti-inflammatory agent, has been used to further inhibit the local inflammatory response [19,20], and angiogenic growth factors, such as vascular endothelial growth factor (VEGF), have been administered to increase the vascularity around the biosensor [21–24].

* Corresponding author. Tel.: +1 617 258 8224; fax: +1 617 324 4323.
E-mail address: strano@mit.edu (M.S. Strano).

0142-9612/$ – see front matter © 2008 Elsevier Ltd. All rights reserved.
doi:10.1016/j.biomaterials.2008.09.052

Individual or dual, concurrent release of DX and VEGF from biosensor hydrogel coatings has been used in previous studies to produce a local environment favorable for biosensor performance [24–27]. Simultaneous delivery of these agents proved to be successful in suppressing tissue inflammation and inducing angiogenesis [25]; however, the counteraction of the pharmacological effects of DX and VEGF has often been ignored. It has been reported that DX constricts vasculature growth [28,29], while the presence of the exogenous protein VEGF triggers an immune response and attracts inflammatory cells [30]. The development of a more efficient strategy of utilizing these agents (e.g. the sequence of delivery) is investigated in this study.

We hypothesized that, compared to the simultaneous delivery of the two tissue response modifiers, sequential delivery of DX, followed by VEGF, would mitigate the pharmacological counteraction, and therefore allow a more effective inhibition of the *in vivo* inflammatory response while concomitantly increasing the vascular network around a biosensor implant. We examined this hypothesis using a microdialysis capillary-based, sensor architecture proposed by ourselves and others [1,7,31]. The sequential delivery method was conducted by an initial, bolus addition of DX delivered directly to the implant site following implantation. Meanwhile, VEGF that had been encapsulated inside the porous, polyethylene glycol (PEG) hydrogel coating was continuously released into the vicinity of the capillary implant.

To evaluate the *in vivo* tissue response, we used the chorioallantoic membrane (CAM) of a developing, ex ova chicken embryo. The avian CAM is the outermost extra-embryonic membrane lining the inner surface of the eggshell, and serves as a support for respiratory and nutrient transport capillaries. The CAM demonstrates immune responses similar to those of mammalian models and facilitates monitoring of vascularization [32,33]. The CAM has been used to test the function of *in vivo* biosensors [34], and study the biocompatibility of biomaterial implants [35], tissue engineering constructs [36,37], and VEGF-induced endothelial cell proliferation [38]. It can serve as a simple and rapid initial screening tool before performing further studies in more complex systems (e.g. mammalian models). Using the CAM tissue-model, we examined the impact of the individual, simultaneous, and sequential delivery of DX and VEGF on the localized immune response and vascular network formation around microdialysis capillary-based, model biosensor implants.

2. Materials and methods

2.1. Preparation of hydrogel prepolymer solution

The pregelled polymer solution (prepolymer solution) was prepared by diluting 1 ml of polyethylene glycol-*n*-diacrylate ($n = 400$) (Polysciences) with 1 ml of deionized (DI) water. The polymer was crosslinked with 30 μl of 2-hydroxy-2-methylpropiophenone (97%) (Sigma). The prepolymer solution was then filtered through a 0.2-μm nylon filter to ensure sterility prior to capillary coating.

2.2. Microdialysis capillary hydrogel coating

In vivo microdialysis hollow fiber capillaries (13 kD MWCO, 200 μm ID, Spectrum Laboratories) were sterilized using UV radiation. Each capillary was inserted inside a miniature glass tube (300 μm OD, Charles Supper Company), and the prepolymer solution was injected into the space between the outer surface of the capillary and the inner surface of the glass tube. The glass tube was immediately placed inside a Jelight Chip Eraser UV chamber (Jelight) to initiate the polymerization reaction. After approximately 2 min of UV exposure (50 $\mu W/cm^2$) to allow the prepolymer solution to congeal, the PEG-coated capillary was pulled out of the glass tube, cut into 1 cm length pieces, and sealed with glue at both ends. Capillary cross-sections were viewed using a microscope; a uniform, PEG coating of an average thickness of 20 μm was observed, whereas no hydrogel was found inside the capillary.

2.3. VEGF and DX addition into hydrogel prepolymer solution

The concentration of $VEGF_{165}$ (Invitrogen) and dexamethasone (Sigma) inside the prepolymer solution was approximately 80 μg/ml and 1.875 mg/ml, respectively. The hydrogel coating procedure using the drug-loaded prepolymer solution was the same as described above.

2.4. VEGF and DX in vitro controlled-release study

A controlled-release study was performed to obtain the in vitro release profiles of VEGF and DX from the capillary hydrogel coating. Capillaries (200 μm ID, 1 cm length) were coated with PEG (~20 μm PEG coating) with the same VEGF or DX prepolymer solution concentrations mentioned above. Each capillary was placed in a 1.5-ml Eppendorf polypropylene microcentrifuge tube with 1 ml aliquot of release buffer (PBS, 0.1% sodium azide). The tubes were placed in a 37 °C shaker incubator rotating at 50 rpm. Daily samples were taken by completely removing the release buffer from each tube and replacing with fresh release buffer. The in vitro release study was continued for up to 8 days. All samples were stored at −20 °C until analysis.

The concentration of VEGF in the release buffer was determined using the Coomassie (Bradford) protein concentration assay kit (Pierce). First, a series of known concentrations of Bovine Serum Albumin (BSA) were prepared as standards. Using a UV spectrometer (UV-3101 UV–vis–nIR spectrophotometer, Shimadzu), the absorbance of the corresponding BSA standards was measured at 595 nm. DI water was used as a blank, and the reading of PBS alone was subtracted from the reading for the samples. A standard calibration curve for VEGF was plotted to define a quantitative relationship between the concentration of VEGF and its observed absorbance. The absorbance of the release buffer samples was measured and the concentrations were calculated using the calibration curve.

The concentration of released DX was detected using the characteristic absorbance of DX at 242 nm. A standard calibration curve was first established using DX at a series of known concentrations. The absorbance readings of the DX standards and release buffer samples were taken at 242 nm.

2.5. Ex ova chicken embryo culture

Fertilized chicken eggs (Hy-Line W-36) were obtained from the University of Illinois Poultry Farm (Urbana, IL). Initially, the eggs were placed horizontally inside an incubator at 38 °C and 65% humidity. After 3 days of incubation, the embryos were transferred into a shell-less embryo culture system (see Supplemental Data section for detailed protocol). Once transfer of the egg contents was complete, the culture system was placed into an incubator at 38 °C and 90% humidity for an additional 4 days (day 7 gestation) before implantation of test samples.

2.6. Bolus addition of DX onto CAM implant site

A 1-μg sample of DX was vigorously mixed with a 500-μl aliquot of PBS inside a 1.5-ml microcentrifuge tube until a homogenous, white solution was observed. For the bolus addition of DX during the initial stage of sequential delivery, a micropipettor was used to dispense the entire DX solution directly onto the CAM implant site following implantation.

2.7. Implantation of test samples into CAM

Polyester thread, non-coated capillary, and PEG-coated capillary of identical length were implanted into the CAM to test their biocompatibility and to observe the host's *in vivo* response toward the implant. The PEG-coated capillary implants were classified into five treatment groups based on the content of the hydrogel coating and drug delivery method: 1) no drugs, 2) VEGF, 3) DX, 4) both VEGF and DX for simultaneous delivery, and 5) VEGF coupled with an initial, bolus addition of 1 μg DX for sequential delivery.

The implantation of the test sample into the CAM was done as previously shown [32]. On day 7 of gestation, the shell-less culture system holding the egg contents was taken out of the incubator and placed inside a laminar flow hood. The Petri dish cover was removed, and the test sample was placed directly on top of the CAM, allowing it to slowly absorb into the tissue. Each implant was observed to have progressively incorporated into the CAM after the first day in contact with the tissue. Before implantation, each test material was dipped in egg white albumin to enhance the incorporation into the CAM [34]. Once the test sample was set onto the CAM, the culture system was covered and placed back into the incubator for 8 more days. Gross evaluations and histological analysis of the resulting CAM were made after the 8-day implantation period (day 15 of gestation).

2.8. Preparation of CAM tissue for histological analysis

Histological evaluation on the CAM specimens was performed 8 days post-placement of the test samples. On the eighth day of ex ova culture, the embryos were fixed in situ with 10% neutral buffered formalin (NBF) solution (4% formaldehyde, Sigma). After 20 h of formalin fixation, a 1 cm × 1 cm sample of CAM tissue, with the implant material in the center, was cut from the entire CAM with suture scissors. The sample tissue was then processed for paraffin embedding, sectioning, and histological staining. Standard protocols of hematoxylin and eosin (H&E) and α-smooth

muscle actin (αSMA) staining were used to quantify the presence of inflammatory cells and blood vessel formation, respectively, near the surface of the implants.

2.9. SEM evaluation of biofouling on implant surface

After formalin fixation, the thread, non-coated capillary, and PEG-coated capillary were carefully removed from the CAM. The extent of fouling of biological milieu on the implant surface was evaluated using a Scanning Electron Microscope (S4700 SEM, Hitachi). SEM images of the surface of each test sample were taken using standard electron microscopy techniques.

2.10. Imaging SWNT inside capillary

Single-walled carbon nanotubes (Southwest Nanotechnologies) wrapped in $(GT)_{15}$ base pair DNA (Integrated DNA Technologies) were prepared using previously published methods [39] and were used to fill a microdialysis capillary. The capillary was implanted in the CAM and after an 8-day implantation period the tissue was fixed in formalin and the SWNT-filled capillary and tissue surrounding the capillary were imaged using a Kaiser Optical Holospec f/1.8 imaging spectrograph attached to a Leica DMPL microscope with 785 nm laser excitation.

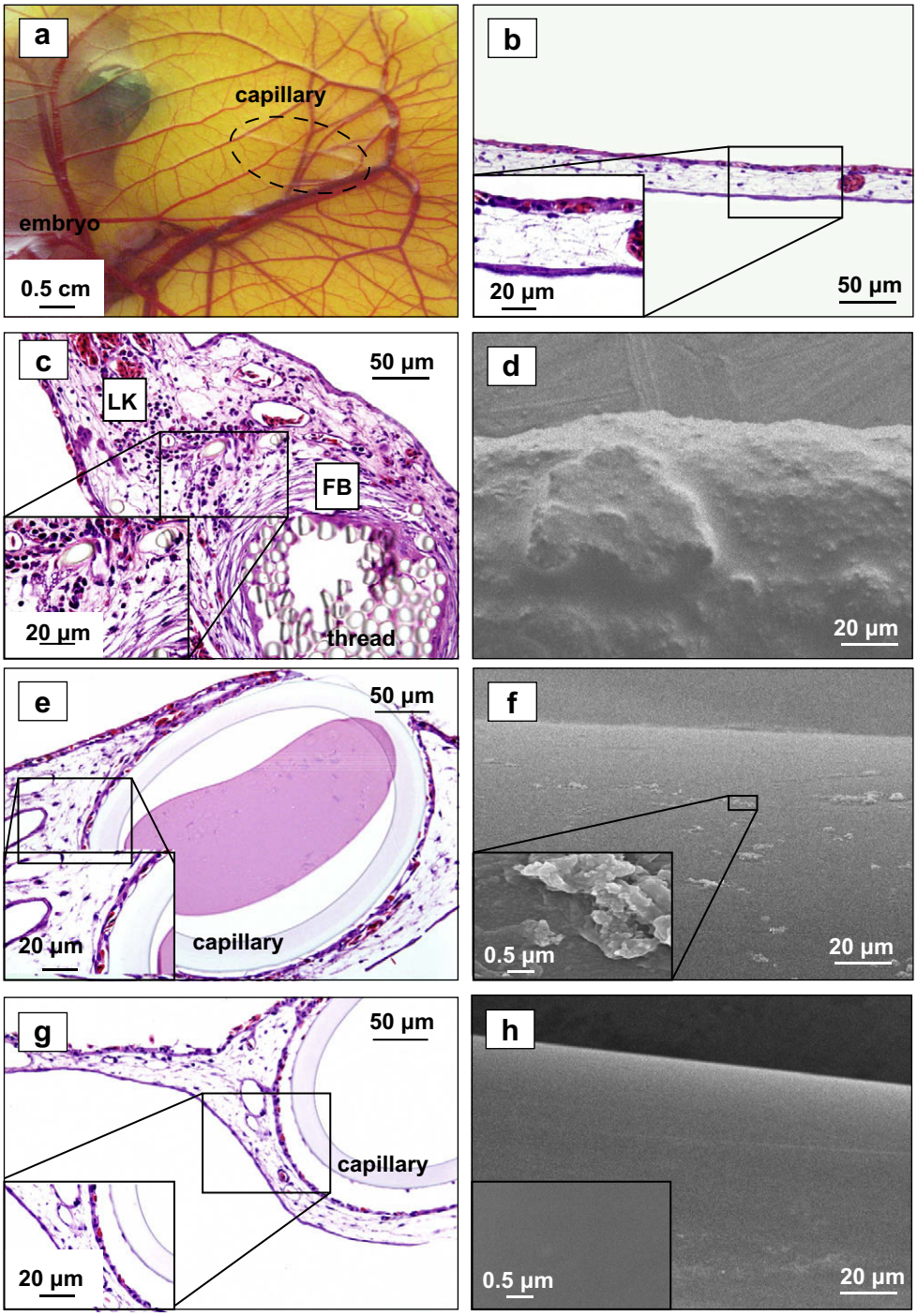

Fig. 1. H&E-stained CAM cross-section images showing immune response to polyester thread, non-coated capillary, and PEG-coated capillary after 8-day implantation, with respective SEM images of the surface of each implant. (a) Gross photograph of chick embryo CAM with embedded capillary. (b) H&E image of normal CAM morphology. (c) H&E image of thread inside CAM, which induced a severe immune response and fibroblast encapsulation, LK – Leukocytes (mostly macrophages and heterophils); FB – fibroblast encapsulation. (d) SEM image of thread surface shows extensive biofouling. (e) H&E image of non-coated capillary, with inflammatory cells and CAM tissue adsorption surrounding the implant. (f) SEM image of non-coated capillary surface with noticeable fouling of adhering proteins. (g) H&E image of PEG-coated capillary. Although a minor immune response was induced, the CAM tissue did not adhere to the hydrogel surface. (h) SEM image of PEG-coated capillary surface shows no biofouling occurred on the hydrogel surface.

For SWNT fluorescence imaging through tissue, diameter sorted sodium cholate suspended SWNT were prepared using previously published methods [40]. Fractions enriched in the smallest diameter nanotubes were used to fill a small glass capillary (~1 mm diameter) which was then inserted subdermally in a Sprague-Dawley rat that had been euthanized by exposure to CO_2. Animal care and euthanasia were performed following animal protocol number 05205 approved by the UIUC IACUC. The SWNT-filled capillary was imaged using a CRI-Maestro *in vivo* imaging system with excitation from 649 to 690 nm and emission measured from 800 to 900 nm with 5 s exposure and 10 accumulations.

2.11. Average inflammatory cell density to assess immune response

CAM tissues embedding the test samples were stained with a standard hematoxylin and eosin (H&E) dye. For each treatment group, cross-sections within 200 μm of the implant surface were examined to obtain the inflammatory cell (heterophils, macrophages) density at ×40 and ×100 magnifications (BX51WI Fixed Stage Microscope, Olympus). Inflammatory cell density was found by counting the number of inflammatory cells, and normalized by the area of interest. The cell count and cross-section area were found using ImageJ (software available for free at rsb.info.nih.gov/ij/). The average inflammatory cell density was reported for each treatment group.

2.12. Average blood vessel density to quantify vasculature growth

A standard α-smooth muscle actin (α-SMA) dye was used to stain CAM tissues embedding the test samples. To obtain blood vessel density within 200 μm of the implant surface, implant cross-sections were analyzed by counting the number of vessels whose smooth muscle layers were stained positive, and averaged over the area. As described above, a light microscope and ImageJ were used for analysis. The average blood vessel density was reported for each treatment group.

2.13. Statistical analysis of histology data

Histology data was represented quantitatively as two main categories: average inflammatory cell density and average blood vessel density, with error bars representing the standard deviation. One-Way Analysis of Variance (ANOVA) was used to determine statistical significance of the data, and Tukey's Post Hoc HSD test was applied to all pair-wise differences between means. Data was considered significant for p values < 0.05.

3. Results and discussion

3.1. In vivo *tissue response to thread, non-coated capillary, and PEG-coated capillary implants*

The biocompatibility of a PEG-coated, micro-capillary implant was evaluated using the CAM tissue-model. For comparison, the *in vivo* tissue response to a polyester thread and a bare, non-coated capillary implant were also examined. Polyester thread was previously shown to have poor biocompatibility inside the CAM [32], whereas the non-coated capillary is known to have a more biocompatible interface, due to the hydrophilicity of the regenerated cellulose surface [41]. The developing chicken embryo CAM was used as an initial screening tool to evaluate the tissue reaction toward each implant. After an 8-day implantation period, the biocompatibility of these implants was assessed using histology (H&E) images of CAM cross-sections, and SEM images of the surface of each implant (Fig. 1). The photograph in Fig. 1a shows an overview of the CAM with a capillary implant on the eighth day of implantation, allowing a direct visualization of the vasculature around the implant site. In the cross-section image of normal CAM (Fig. 1b), very few inflammatory cells (mostly macrophages and heterophils identified by H&E dye) were observed. In contrast, a much higher presence of inflammatory cells, fibroblast encapsulation, and swelling (edema) were

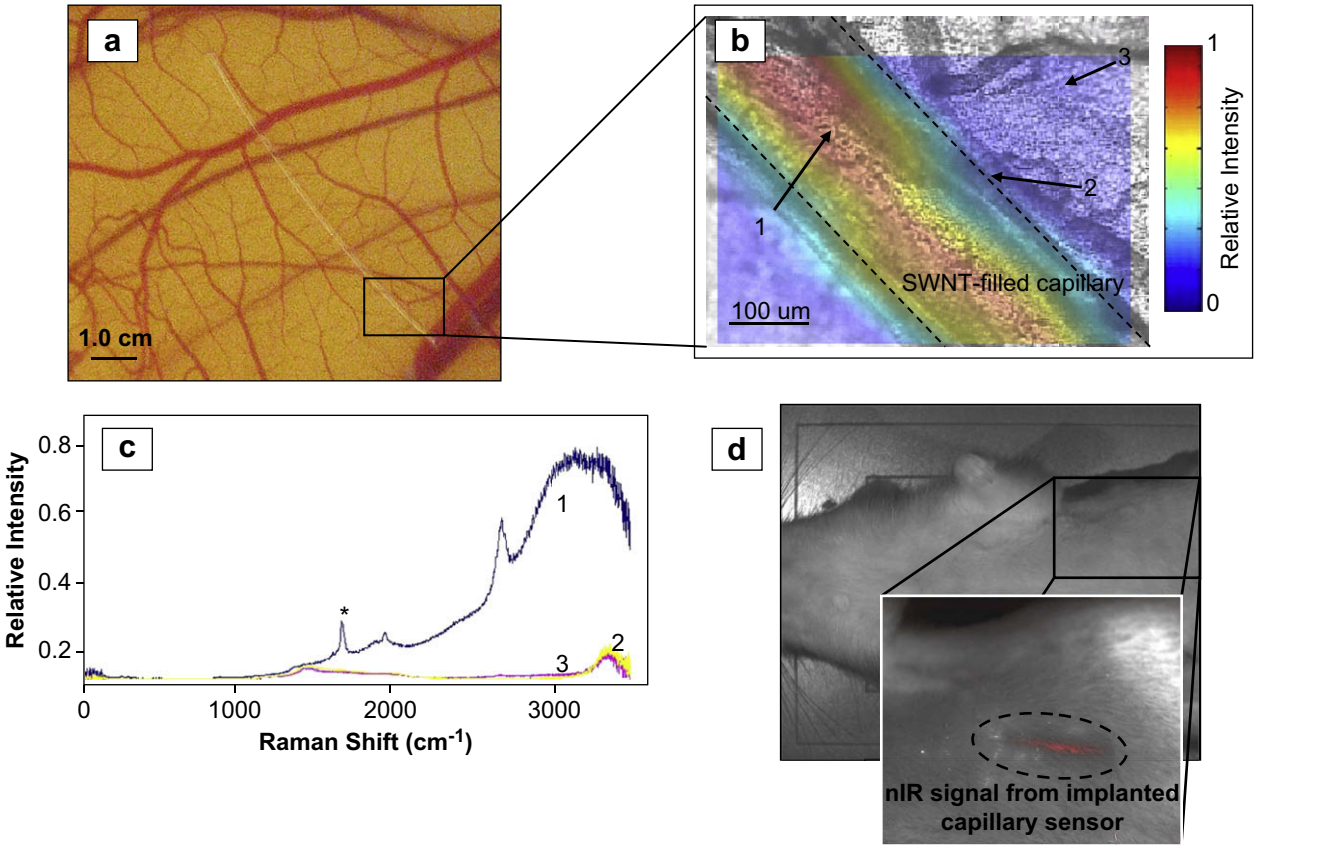

Fig. 2. Micrograph of a non-coated capillary containing DNA-encapsulated nanotubes incorporated into CAM tissue, with corresponding Raman spectra G-band intensity (*) area map and intensity spectra. (a) Photograph of fully incorporated capillary after 8 days post-placement onto CAM (gestation day 15). (b) Area map of Raman 1592 cm^{-1} G-band intensity of nanotubes inside capillary overlaid onto an optical micrograph of the same region. Location points indicate inside and around the SWNT-filled capillary implant. (c) Raman G-band intensity spectra of selected location points 1, 2, and 3 of area map in (b). Absence of a 1592 cm^{-1} Raman peak in points 2 and 3 suggests minimal SWNT content. (d) A sealed capillary loaded with SWNT was placed beneath the skin of a rat. The capillary was imaged with excitation from 649 to 690 nm and emission collected from 800 to 900 nm. Fluorescence of SWNT is clearly visible through the tissue.

found in the tissue surrounding the thread implant (Fig. 1c). As shown in the post-implantation SEM image (Fig. 1d), the surface of the thread was extensively covered with adhering proteins and other biological milieu. The bare capillary resulted in a minor immune response, while CAM tissue strongly adhered to the implant surface (Fig. 1e). The corresponding SEM image shows pieces of tissue remaining on the capillary (Fig. 1f). The PEG-coated implant induced an immune response similar to that found near the non-coated capillary (Fig. 1g), which shows that the surface material of both platforms (regenerated cellulose and PEG) have higher biocompatibility than the rough, polyester thread. However, in contrast to the case of the bare capillary, CAM tissue did not adsorb onto implants with a PEG-coated surface (Fig. 1g), and biofouling was not observed in the SEM image (Fig. 1h). In support of these histology and SEM image observations, the inflammatory cell density (cell number $\times 10^3/\mu m^2$) within 200 μm of the implant surface was quantified for the thread, non-coated capillary, and PEG-coated capillary implants (Supplemental Fig. 1). Overall, we have shown the PEG-coated capillary ensures minimal immune response and biofouling onto its surface, which is crucial for proper *in vivo* biosensor performance. These results are supported by other studies in the literature [42–44].

3.2. Visualization of SWNT in the CAM model and through tissue

An injection of DNA-wrapped SWNT to the CAM led to the highest inflammatory cell density among all treatment groups (Supplemental Fig. 1). To verify that the proposed microdialysis capillary-based sensor architecture would effectively prevent SWNT leaching into the surrounding tissue, DNA-wrapped SWNT-filled capillaries were implanted in a CAM model for 8 days (Fig. 2a). After fixation, the tissue surrounding the SWNT-filled capillary was imaged using a micro-Raman spectrometer. Characteristic SWNT Raman features were only visible inside the capillary, while tissue immediately surrounding and several microns away did not show the presence of SWNT (Fig. 2b and c). Additionally, the SWNT-filled capillary had an equivalent physiological response as an unfilled capillary used for the sequential delivery experiments (Supplemental Fig. 1).

While SWNT have been used for a number of other biological applications, from drug delivery [45] to cancer therapy [46], to our knowledge no demonstration exists of SWNT fluorescence imaging through tissue. To demonstrate this imaging, small diameter nanotubes, with stronger emission around 900 nm, were filled in a small glass capillary. The capillary was inserted under the skin of a rat and imaged using a CRI-Maestro *in vivo* imaging system (Fig. 1d). The SWNT-filled capillary can clearly be distinguished, demonstrating the potential of a SWNT-based subcutaneous sensor.

3.3. In vitro *release study of dexamethasone and VEGF*

The release rates of VEGF and DX from the capillary hydrogel coating were examined in an in vitro controlled-release study (Fig. 3). The cumulative release profiles of VEGF (Fig. 3a) and DX (Fig. 3b) show the capillaries released ~45 ng of VEGF and ~0.9 μg of DX during the 9-day release period. In preliminary experiments, these drug doses were found to be optimal in inducing a statistically significant tissue response. During day 0–2, 76.5% and 75.7% of the initial loaded amount of VEGF and DX, respectively, had been released. After this time interval, the release rate of both drugs gradually decreased during the remainder of the 8-day collection period. Complete depletion of DX in the hydrogel coating occurred around day 6.

To model the relationship between drug depletion and release rate, the two release profiles were fit to a first-order, drug release kinetics approximation,

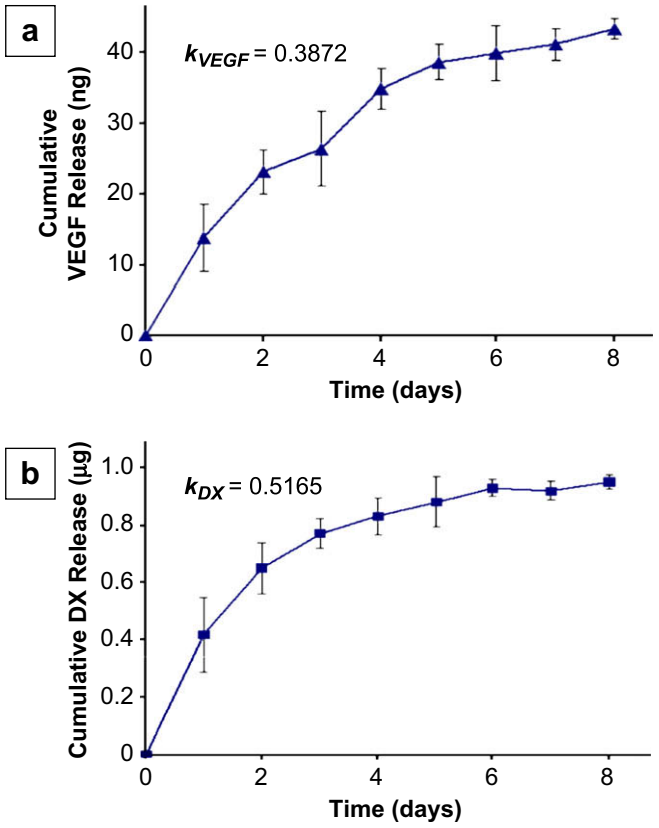

Fig. 3. In vitro release profiles of (a) VEGF ($n = 6$) and (b) DX ($n = 6$) for 8-day collection. By modeling the relationship between drug depletion and release rate using first-order drug release kinetics, DX was found to have a higher release rate constant (k) than VEGF. Data points represent mean cumulative release amount, with error bars representing standard deviation from the mean.

$$\frac{C_{\text{drug}}}{C_{\text{drug},0}} = e^{-kt} \tag{1}$$

where C_{drug} is the drug concentration remaining in the hydrogel coating, $C_{\text{drug},0}$ represents the initial amount of drug encapsulated, and k is the drug release rate constant (day^{-1}). The rate constant (k) in Eq. (1) was quantified by fitting the drug concentration (C_{drug}) over time (t) using a least-squares linear regression approach. Solving for k, the rate constants for VEGF and DX were 0.4/day and 0.5/day, respectively. C_{Dx} was found to deplete more rapidly inside the hydrogel layer than C_{VEGF}, leading to its higher value of k. DX is an anti-inflammatory steroid with a molecular weight of 392 g/mol, while VEGF_{165} is a 38.6-kDa macromolecule protein. Therefore, the apparent difference in release profile and k is assumed to be due to the difference in molecular size and subsequent diffusivity through the crosslinked PEG coating.

3.4. Vascular network formation in response to VEGF bolus addition and controlled-release

It has been shown in previous studies that increased vascularity (using VEGF) around an implantable biosensor can improve its performance and lifetime [22,23]. Two VEGF delivery methods were proposed: a single, bolus addition of VEGF onto the implant site, simulating an injection of VEGF to the site of the sensor in a mammalian model, and a sustained-release of VEGF from the PEG coating of the capillary implant. In Fig. 4, the local vascular network formed using the two delivery methods was compared to that around the VEGF-empty PEG-coated implant (control). Around the control, no angiogenic activity was observed after the 8-day

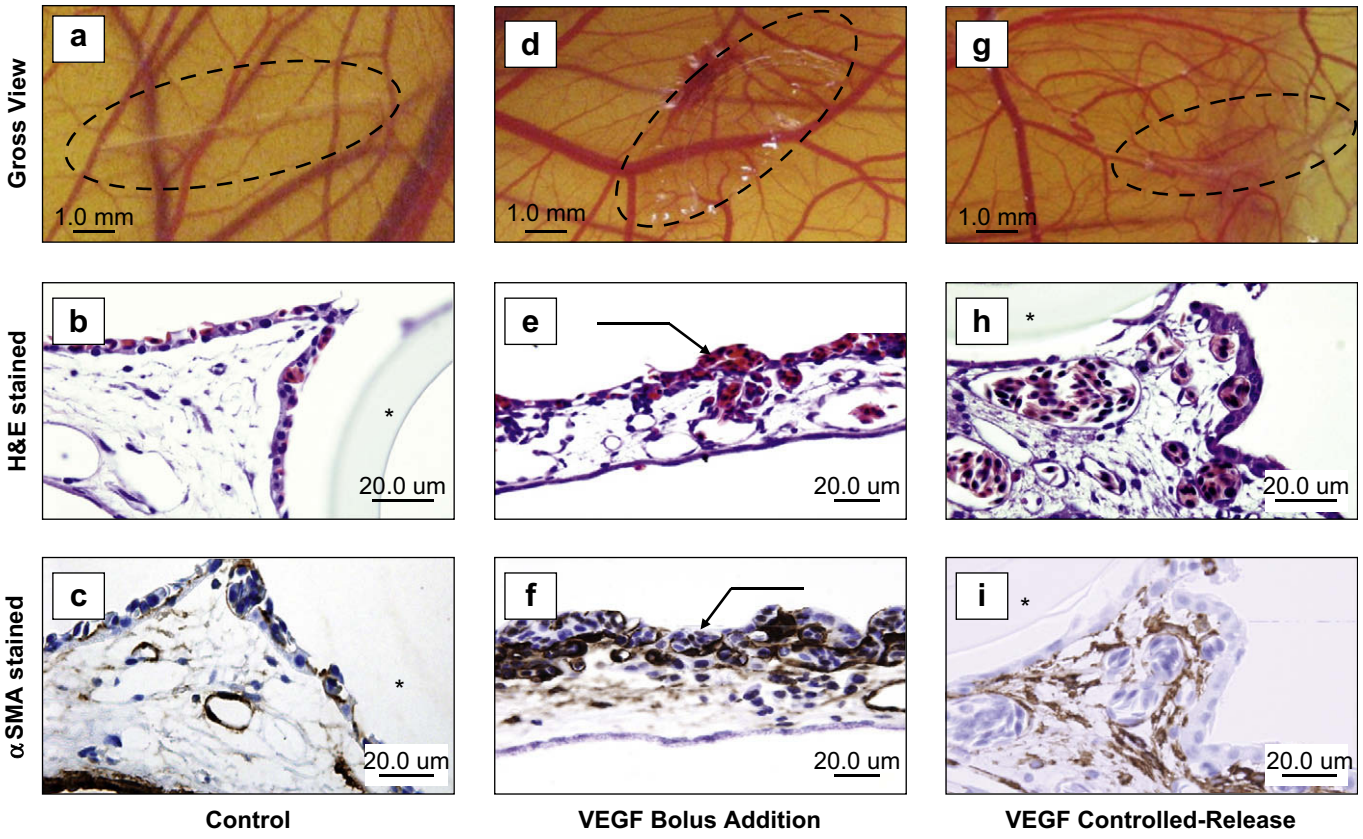

Fig. 4. Gross photograph, and H&E/αSMA-stained cross-section images of CAM embedding a capillary implant with (a, b, c) drug-empty PEG coating; (d, e, f) localized, bolus addition of 5 μg VEGF; and (g, h, i) VEGF-releasing PEG coating (80 μg/mL) for an 8-day implantation period (gestation day 15). (a, b, c): Around the drug-empty PEG coating, neither a significant inflammatory response nor sprouting of new vasculature was observed. (d, e, f): The bolus addition of VEGF-induced localized angiogenesis emerging from pre-existing arteries, and the formation of abnormal vasculature directly below the chorionic epithelium. (g, h, i): VEGF-controlled release from the PEG coating induced the development of a fine vasculature network with a wide distribution of blood vessel size. Asterisk (*) indicates position of implant in image.

implantation period (Fig. 4a). H&E and αSMA stained cross-sections show neither a significant inflammatory response nor sprouting of new vasculature (Fig. 4b and c). Eight days after the addition of approximately 5 μg of VEGF onto the implant site, the induced localized angiogenic response led to the formation of enlarged blood vessels emerging from pre-existing arteries (Fig. 4d). Histology results show a higher number of inflammatory cells present in the CAM compared to the control (Fig. 4e). The bolus addition of VEGF induced an uncontrolled, non-uniform, and clustered growth of blood vessels (Fig. 4f). Vasculature growth was concentrated directly below the chorionic epithelium, and was limited to a small area around the bolus addition site. Such lack of a uniform, dense vasculature network would not be ideal for sensor performance.

The controlled-release of VEGF led to the formation of a non-clustered, broad distribution of blood vessels around the capillary implant (Fig. 4 g). H&E-stained image shows a higher presence of inflammatory cells in the CAM than in the control (Fig. 4h), while the αSMA stained image shows the development of a vasculature network with a wider range of blood vessel size (Fig. 4i). In contrast to the bolus addition case, a slow and steady release of VEGF from the hydrogel coating had stimulated the distant vasculature into growing toward the VEGF source. This higher degree of angiogenesis is necessary for increased, steady-state levels of analyte flux to the nearby region of the sensor, but it is also necessary to limit the inflammatory response stimulated by VEGF.

3.5. Histological analysis (H&E) of tissue immune response

An initial delivery of an anti-inflammatory agent (DX), followed by a continuous release of an angiogenesis stimulant (VEGF) from the hydrogel coating, was performed to promote neovascularization around the biosensor platform while modifying tissue inflammation. The efficacy of sequential drug treatment was examined using histological analysis of five treatment groups: a capillary with a PEG coating containing 1) no drugs, 2) VEGF for controlled-release, 3) DX for controlled-release, 4) both VEGF and DX for simultaneous delivery, and 5) VEGF coupled with a bolus addition of DX at the implant site for sequential treatment. H&E-stained cross-sections of CAM with the embedded implant are shown in Fig. 5a–e. The inflammatory cell density (cell number $\times 10^3/\mu m^2$) within 200 μm of the implant surface was examined for each treatment group (Fig. 5f). Relative to the treatment group with no drugs embedded in the PEG coating (control) ($2.07 \pm 0.68 \times 10^{-3}/\mu m^2$), the sustained-release of VEGF resulted in a higher inflammatory cell density ($3.05 \pm 0.35 \times 10^{-3}/\mu m^2$), whereas DX sustained-release resulted in a lower value ($0.97 \pm 0.24 \times 10^{-3}/\mu m^2$). The dual, concurrent and sequential delivery of the two agents both decreased the inflammatory cell density ($1.52 \pm 0.21 \times 10^{-3}/\mu m^2$ and $1.06 \pm 0.07 \times 10^{-3}/\mu m^2$, respectively) in the vicinity of the implant compared to the control, but only the result of the sequential treatment was statistically significant. The average inflammatory cell density of the sequential treatment was 30.3% lower than that of the simultaneous delivery. The counteractive effect of inflammatory cell attraction of VEGF and immune response suppression of DX during concurrent delivery may have contributed to the smaller decrease in local immune response relative to the control. This shows the limitation of simultaneous administration, hinting at the need for sequential release.

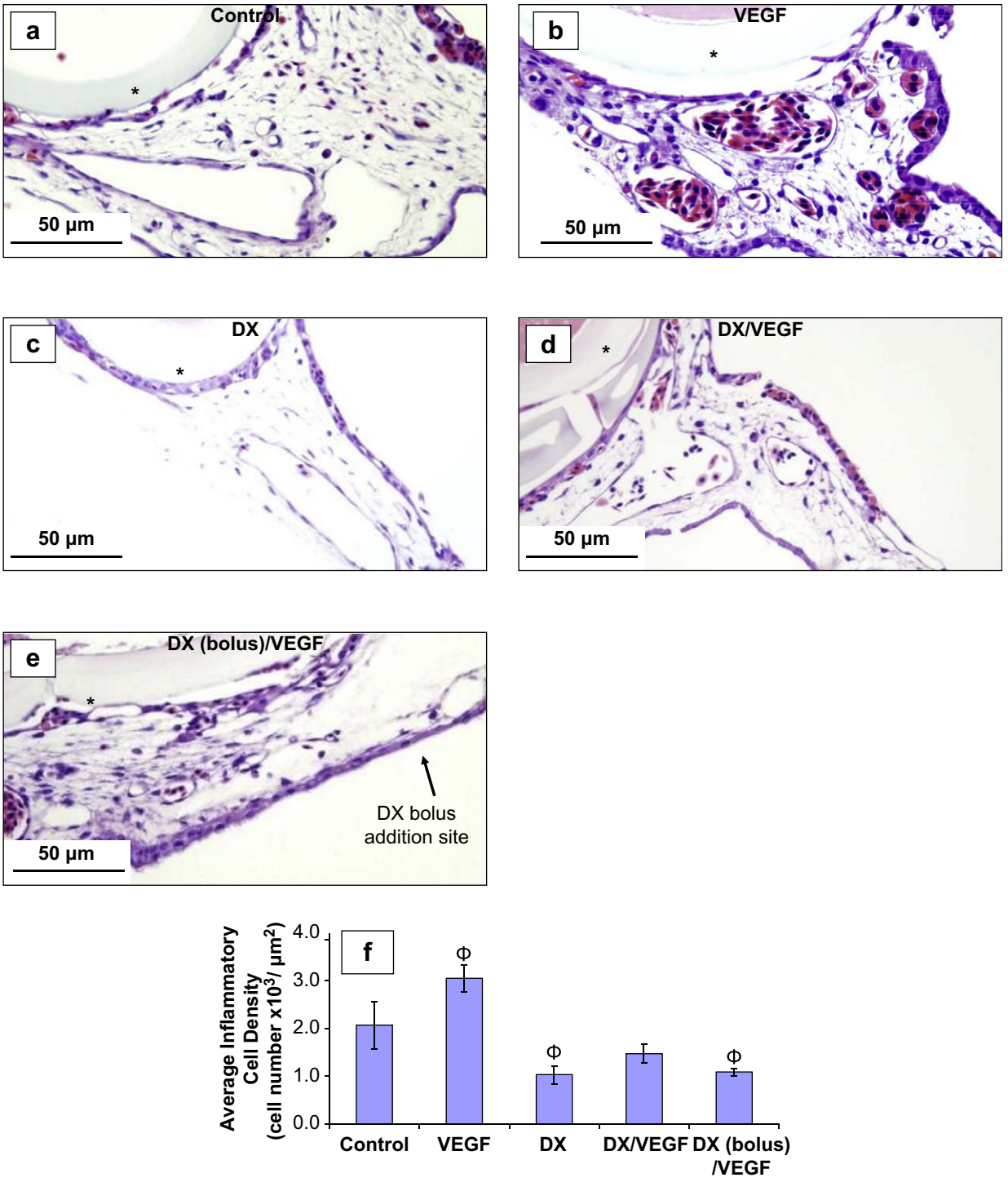

Fig. 5. H&E-stained CAM cross-sections embedding a capillary implant with PEG coating releasing: (a) no drugs; (b) VEGF; (c) DX; (d) both VEGF and DX; and (e) VEGF coupled with a bolus addition of 1 μg DX (arrow). Asterisk (*) indicates position of implant in image. (f) The average inflammatory cell density within 200 μm of implant was quantified for each treatment group. Φ indicates statistical significance relative to the control ($p < 0.05$).

3.6. Histological analysis (αSMA) of vascular network formation

Cross-sections of αSMA-stained CAM for each of the five treatment groups are shown in Fig. 6a–e. Average vasculature density (blood vessel number $\times 10^3/\mu m^2$) within 200 μm of the implant surface is shown in Fig. 6f. The controlled-release of both VEGF and DX ($1.24 \pm 0.35 \times 10^{-3}/\mu m^2$) and VEGF coupled to an initial, bolus addition of DX ($1.15 \pm 0.30 \times 10^{-3}/\mu m^2$), led to higher vasculature formation than the control group ($0.71 \pm 0.20 \times 10^{-3}/\mu m^2$) and DX controlled-release ($0.44 \pm 0.19 \times 10^{-3}/\mu m^2$). However, compared to VEGF delivery alone ($1.98 \pm 0.21 \times 10^{-3}/\mu m^2$), both methods had a significant decrease in vasculature growth. This confirms that the VEGF-DX interaction can lead to opposite outcomes: VEGF counteracts the anti-inflammatory action of DX, while the latter inhibits VEGF-induced tissue vascularization. The average vasculature density resulting from dual, concurrent treatment and sequential treatment was statistically the same, which shows that prior bolus delivery of DX does not necessarily provide better performance

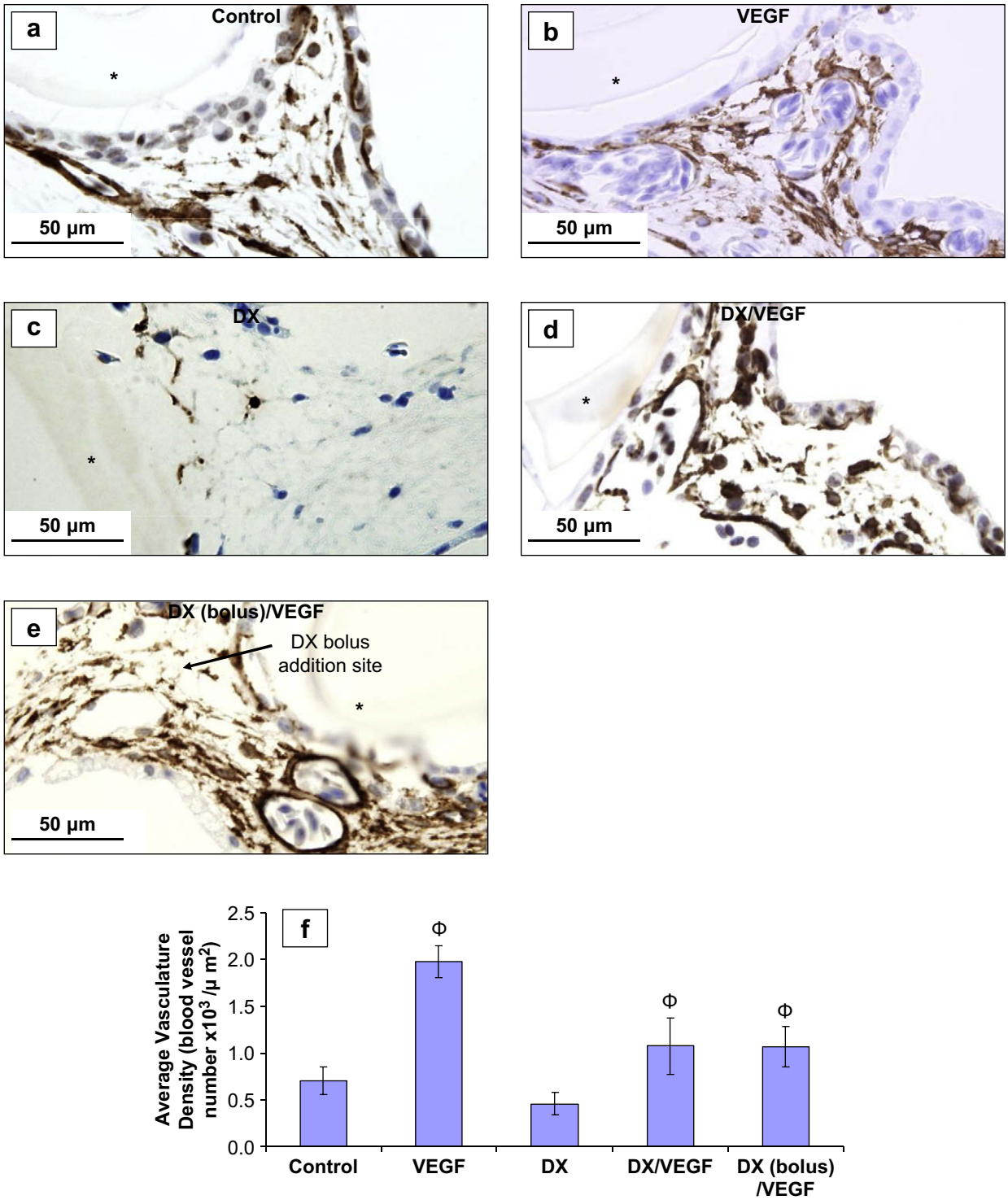

Fig. 6. αSMA-stained CAM cross-sections embedding a capillary implant with PEG coating releasing: (a) no drugs; (b) VEGF; (c) DX; (d) both VEGF and DX; and (e) VEGF coupled with a bolus addition of 1 μg DX (arrow). Asterisk (*) indicates position of implant in image. (f) The average vasculature density within 200 μm of implant was quantified for each treatment group. Φ indicates statistical significance relative to the control ($p < 0.05$).

(i.e. more tissue vascularization) over simultaneous delivery. Therefore, this aspect of controlling the local tissue response remains to be further improved.

The effects of DX and VEGF may counteract each other, and therefore what is of interest is a therapeutic index that measures an increase in vasculature given a simultaneous inflammatory response. We define the index as the ratio of average vasculature density to average inflammatory cell density for each treatment group based on the quantitative results from the above histological analyses (Fig. 7). The index reflects how well the drug delivery method (individual, simultaneous, or sequential) promotes localized angiogenesis against the host's immune response.

Fig. 7 shows that the controlled-release of VEGF, simultaneous DX/VEGF delivery, and sequential DX/VEGF delivery groups had significantly higher indices than those of the control and DX controlled-release groups. Relative to the control (0.38 ± 0.06), the VEGF-controlled-release group resulted in a higher index (0.66 ± 0.10) due to the drug-induced increase in local vasculature.

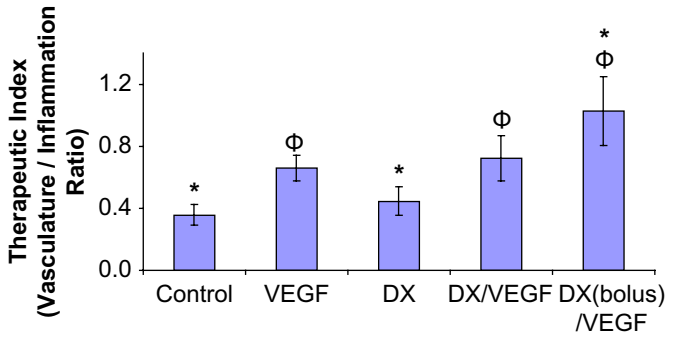

Fig. 7. The therapeutic index, defined as the ratio of average vasculature density to average inflammatory cell density, was quantified for each treatment group. Among the treatment groups, sustained-release of VEGF coupled with a bolus addition of DX, led to the highest index. Φ indicates statistical significance relative to the control ($p < 0.05$); * indicates statistical significance relative to VEGF + DX ($p < 0.05$).

However, this higher value was limited due to the elevated number of inflammatory cells triggered by the sustained presence of the exogenous protein. DX controlled-release from the capillary PEG coating led to the decrease in both vasculature and immune response, and the index of this group was found to be statistically similar to that of the control (0.44 ± 0.10). Our results indicate that the therapeutic index resulting from sequential DX/VEGF delivery (1.05 ± 0.13) was 60.3% higher than that of VEGF delivery, and 139.3% higher than that of DX release. Furthermore, this index was a 32.1% increase compared to that of simultaneous administration of these agents (0.80 ± 0.14), showing that DX/VEGF sequential delivery provided the highest therapeutic index among the five experimental groups.

As the capillary is set onto the CAM and is gradually embedded, the implant is immediately detected by the host's immune system and triggers an inflammatory response. In the case of an *in vivo* biosensor, inflammation and blood vessel regression caused by fibroblast encapsulation during the wound-healing process disrupts analyte transport to the sensor surface, resulting in loss of accuracy and function, as well as increased measurement lag time. As the initial, physiological response becomes stabilized and inflammation progresses onto its later stages, collagen and vasculature remodeling occur around the capillary implant. To target the events of this later timeframe, a sustained-release of VEGF from the implant coating was applied to facilitate tissue regeneration, producing an abundant, yet highly organized blood vessel network around the capillary. In the application of DX and VEGF, the order of delivery of these tissue response modifiers is highly critical for engineering of tissue structure due to their opposite pharmacological effects. In the sequential delivery of DX and VEGF, the initial application of DX mediates the early immune response by reducing the population of inflammatory cells before VEGF-induced angiogenesis. We note that DX may still remain in the tissue stroma during VEGF release, which may deteriorate the bioactivity of VEGF. Therefore, the pharmacological counteraction of the two drugs may not be completely avoided. However, our results suggest that sequential delivery can overcome the counteractive effects of DX on VEGF seen during simultaneous administration, allowing a more effective inhibition of the inflammatory response while concomitantly increasing the vascular network around the capillary implant. Hence, the proposed sequential treatment proved to be an effective strategy in the development of a local *in vivo* environment favorable for long-term, accurate biosensor performance.

4. Conclusion

In this study, we examined the *in vivo* pharmacological effects of the sequential delivery of DX and VEGF around a hydrogel-coated, microdialysis capillary implant in the CAM tissue-model. We demonstrated that such a capillary is suitable for use for an SWNT-based fluorescence sensor and also demonstrated SWNT fluorescence detection through tissue. The hydrogel coating effectively minimized *in vivo* protein and cell adhesion, as well as fibroblast encapsulation, while showing a comparable inflammatory response with the bare implant. Controlled-release of VEGF led to the formation of a more uniform, broader distribution of blood vessels around the capillary implant than bolus VEGF delivery. The sequential delivery of DX followed by VEGF resulted in a highest level of vasculature around the implant for a given amount of inflammation. This result proves to be a more effective drug delivery technique than simultaneous delivery, allowing us to reduce the immune response and develop a well-vascularized environment favorable for biosensor performance.

Acknowledgments

This work was funded by the NSF CAREER award to MSS and a Beckman Young Investigator Award, also to MSS. PWB gratefully acknowledges support from the School of Chemical Sciences and the Department of Chemical and Biomolecular Engineering at UIUC in the form of the Drickamer Graduate Fellowship. The authors would like to thank J. Chladny, K. Reed, G. Simon, and R. Walker at the Veterinary Diagnostic Histopathology Laboratory at the College of Veterinary Medicine (UIUC) for H&E and αSMA histology staining of the CAM tissue. The authors would also like to thank Prof. M. Wallig of the College of Veterinary Medicine (UIUC) for his assistance in analyzing the histology stains, and Prof. S. Boppart and F. Nguyen (UIUC) for help with capillary implantation in the rat and for use of their CRI-Maestro.

Appendix. Supplementary material

Supplementary data associated with this article can be found in the online version, at doi:10.1016/j.biomaterials.2008.09.052.

Appendix

Figures with essential colour discrimination. Many figures in this article are difficult to interpret in black and white. The full colour images can be found in the on-line version, at doi:10.1016/j.biomaterials.2008.09.052.

References

[1] Barone PW, Baik S, Heller DA, Strano MS. Near-infrared optical sensors based on single-walled carbon nanotubes. Nature Materials 2005;4(1):86–92.
[2] Barone PW, Strano MS. Reversible control of carbon nanotube aggregation for a glucose affinity sensor. Angewandte Chemie – International Edition 2006;45(48):8138–41.
[3] Heller DA, Jeng ES, Yeung TK, Martinez BM, Moll AE, Gastala JB, et al. Optical detection of DNA conformational polymorphism on single-walled carbon nanotubes. Science 2006;311(5760):508–11.
[4] Jeng ES, Moll AE, Roy AC, Gastala JB, Strano MS. Detection of DNA hybridization using the near-infrared band-gap fluorescence of single-walled carbon nanotubes. Nano Letters 2006;3:371–5.
[5] O'Connell MJ, Bachilo SM, Huffman CB, Moore VC, Strano MS, Haroz EH, et al. Band gap fluorescence from individual single-walled carbon nanotubes. Science 2002;297(5581):593–6.
[6] Wray S, Cope M, Delpy DT, Wyatt JS, Reynolds EOR. Characterization of the near-infrared absorption-spectra of cytochrome-Aa3 and hemoglobin for the non-invasive monitoring of cerebral oxygenation. Biochimica Et Biophysica Acta 1988;933(1):184–92.
[7] Barone PW, Parker RS, Strano MS. In vivo fluorescence detection of glucose using a single walled carbon nanotube optical sensor: design, fluorophore properties, advantages and disadvantages. Analytical Chemistry 2005;77(23):7556–62.
[8] Moussy F. Biosensor/tissue interactions. Microtechnologies in medicine and biology, first annual international, conference on 2000. p. 479–82.
[9] Francis Moussy P, Reichert W, May W, May T. Biomaterials community examines biosensor biocompatibility. Diabetes Technology & Therapeutics 2000;2(3).

[10] Frost M, Meyerhoff M. In vivo chemical sensors: tackling biocompatibility. Analytical Chemistry 2006;78(21):7370–7.
[11] Wisniewski N, Moussy F, Reichert W. Characterization of implantable biosensor membrane biofouling. Fresenius' Journal of Analytical Chemistry 2000;366(6):611–21.
[12] Wisniewski N, Klitzman B, Miller B, Reichert W. Decreased analyte transport through implanted membranes: differentiation of biofouling from tissue effects. Journal of Biomedical Materials Research 2001;57(4):513–21.
[13] Sharkawy A, Klitzman B, Truskey G, Reichert W. Engineering the tissue which encapsulates subcutaneous implants. I. Diffusion properties. Journal of Biomedical Materials Research 1997;37(3):401–12.
[14] Gilligan B, Shults M, Rhodes R, Jacobs P, Brauker J, Pintar T, et al. Feasibility of continuous long-term glucose monitoring from a subcutaneous glucose sensor in humans. Diabetes Technology & Therapeutics 2004;6(3):378–86.
[15] Rebrin K, Fischer U, Hahn von dorsche H, Von woetke T, Abel P, Brunstein E. Subcutaneous glucose monitoring by means of electrochemical sensors: fiction or reality? Journal of Biomedical Engineering 1992;14(1):33–40.
[16] Wisniewski N, Reichert M. Methods for reducing biosensor membrane biofouling. Colloids and Surfaces B: Biointerfaces 2000;18(3–4):197–219.
[17] Shin B, Wisniewski N, Reichert W. Water-soluble treatments to enhance glucose permeability of protein-resistant polymer overlayers. Polymer Edition. Journal of Biomaterials Science 2001;12(5):467–77.
[18] Quinn C, Connor R, Heller A. Biocompatible, glucose-permeable hydrogel for in situ coating of implantable biosensors. Biomaterials 1997;18(24): 1665–70.
[19] Kim D, Martin D. Sustained release of dexamethasone from hydrophilic matrices using PLGA nanoparticles for neural drug delivery. Biomaterials 2006;27(15):3031–7.
[20] Hickey T, Kreutzer D, Burgess D, Moussy F. In vivo evaluation of a dexamethasone/PLGA microsphere system designed to suppress the inflammatory tissue response to implantable medical devices. Materials Research 2002; 61:180–7.
[21] Richardson T, Peters M, Ennett A, Mooney D. Polymeric system for dual growth factor delivery. Nature Biotechnology 2001;19(11):1029–34.
[22] Klueh U, Dorsky D, Kreutzer D. Use of vascular endothelial cell growth factor gene transfer to enhance implantable sensor function in vivo. Journal of Biomedical Materials Research 2003;67(4):1072–86.
[23] Klueh U, Dorsky D, Kreutzer D. Enhancement of implantable glucose sensor function in vivo using gene transfer-induced neovascularization. Biomaterials 2005;26(10):1155–63.
[24] Tilakaratne H, Hunter S, Andracki M, Benda J, Rodgers V. Characterizing short-term release and neovascularization potential of multi-protein growth supplement delivered via alginate hollow fiber devices. Biomaterials 2007;28(1):89–98.
[25] Patil S, Papadmitrakopoulos F, Burgess D. Concurrent delivery of dexamethasone and VEGF for localized inflammation control and angiogenesis. Journal of Controlled Release 2007;117(1):68–79.
[26] Norton L, Tegnell E, Toporek S, Reichert W. In vitro characterization of vascular endothelial growth factor and dexamethasone releasing hydrogels for implantable probe coatings. Biomaterials 2005;26(16):3285–97.
[27] Jain N, Vegad J, Katiyar A, Awadhiya R. Effects of anti-inflammatory drugs on increased vascular permeability in acute inflammatory response in the chicken. Avian Pathology 1995;24(4):723–9.
[28] Badruddoja M, Krouwer H, Rand S, Rebro K, Pathak A, Schmainda K. Anti-angiogenic effects of dexamethasone in 9L gliosarcoma assessed by MRI cerebral blood volume maps. Neuro-Oncology 2003;5(4):235–43.
[29] Hoepelman A, Flier M, Coenjaerts F. Dexamethasone downregulates *Cryptococcus neoformans*-induced vascular endothelial growth factor production: a role for corticosteroids in cryptococcal meningitis? JAIDS, Journal of Acquired Immune Deficiency Syndromes 2004;37(3):1431–2.
[30] Ohm J, Carbone D. VEGF as a mediator of tumor-associated immunodeficiency. Immunologic Research 2001;23(2):263–72.
[31] Ballerstadt R, Schultz JS. A fluorescence affinity hollow fiber sensor for continuous transdermal glucose monitoring. Analytical Chemistry 2000; 72(17):4185–92.
[32] Valdes T, Kreutzer D, Moussy F. The chick chorioallantoic membrane as a novel in vivo model for the testing of biomaterials. Journal of Biomedical Materials Research (USA) 2002;62(2):273–82.
[33] Ribatti D, Nico B, Vacca A, Roncali L, Burri P, Djonov V. Chorioallantoic membrane capillary bed: a useful target for studying angiogenesis and anti-angiogenesis in vivo. The Anatomical Record 2001;264(4):317–24.
[34] Valdes T, Klueh U, Kreutzer D, Moussy F. Ex ova chick chorioallantoic membrane as a novel in vivo model for testing biosensors. Journal of Biomedical Materials Research 2003;67A:215–23.
[35] Klueh U, Dorsky D, Moussy F, Kreutzer D. Ex ova chick chorioallantoic membrane as a novel model for evaluation of tissue responses to biomaterials and implants. Journal of Biomedical Materials Research 2003; 67(3):838–43.
[36] Spanel-Borowski K. The chick chorioallantoic membrane as test system for biocompatible materials. Research in Experimental Medicine 1989;189(1): 69–75.
[37] Borges J, Tegtmeier F, Padron N, Mueller M, Lang E, Stark G. Chorioallantoic membrane angiogenesis model for tissue engineering: a new twist on a classic model. Tissue Engineering 2003;9(3):441–50.
[38] Wilting J, Christ B, Bokeloh M, Weich H. In vivo effects of vascular endothelial growth factor on the chicken chorioallantoic membrane. Cell and Tissue Research 1993;274(1):163–72.
[39] Heller DA, Baik S, Eurell TE, Strano MS. Single-walled carbon nanotube spectroscopy in live cells: towards long-term labels and optical sensors. Advanced Materials 2005;17(23):2793.
[40] Arnold MS, Green AA, Hulvat JF, Stupp SI, Hersam MC. Sorting carbon nanotubes by electronic structure using density differentiation. Nature Nanotechnology 2006;1:60–5.
[41] Miyamoto T, Takahashi S, Ito H, Inagaki H, Noishiki Y. Tissue biocompatibility of cellulose and its derivatives. Journal of Biomedical Materials Research 1989;23(1):125–33.
[42] Doretti L, Ferrara D, Gattolin P, Lora S. Covalently immobilized enzymes on biocompatible polymers for amperometric sensor applications. Biosensors and Bioelectronics 1996;11(4):365–73.
[43] Pathak C, Sawhney A, Hubbell J. Rapid photopolymerization of immunoprotective gels in contact with cells and tissue. Journal of the American Chemical Society 1992;114(21):8311–2.
[44] Desai N, Hubbell J. Solution technique to incorporate polyethylene oxide and other water-soluble polymers into surfaces of polymeric biomaterials. Biomaterials 1991;12(2):144–53.
[45] Cai D, Mataraza JM, Qin ZH, Huang ZP, Huang JY, Chiles TC, et al. Highly efficient molecular delivery into mammalian cells using carbon nanotube spearing. Nature Methods 2005;2(6):449–54.
[46] Kam NWS, O'Connell M, Wisdom JA, Dai H. Carbon nanotubes as multifunctional biological transporters and near-infrared agents for selective cancer cell destruction. Proceedings of the National Academy of Sciences of the United States of America 2006;102(33):11600–5.